INSTITUTE OF PHYSICS PUBLISHING JOURNAL OF PHYSICS G: NUCLEAR AND PARTICLE PHYSICS

J. Phys. G: Nucl. Part. Phys. **28** (2002) 2907–2920 PII: S0954-3899(02)52566-4

On the muon–nucleus integrals entering the neutrinoless $\mu^- \to e^-$ conversion rates

T S Kosmas[1,2] **and I E Lagaris**[3]

[1] Theoretical Physics Division, University of Ioannina, GR-45110 Ioannina, Greece
[2] Institut für Theoretische Physik der Universität Tübingen, D-72076 Tübingen, Germany
[3] Department of Computer Science, University of Ioannina, GR-45110 Ioannina, Greece

Received 20 August 2002, in final form 27 September 2002
Published 25 October 2002
Online at stacks.iop.org/JPhysG/28/2907

Abstract

The muon–nucleus integrals which determine the nuclear-structure dependence of the branching ratio $R_{\mu e}$, i.e. the rate of the flavour-changing muon–electron conversion divided by the total rate of the ordinary muon capture, are extensively studied. Precise muon wavefunctions are employed which are obtained by solving the Schrödinger and Dirac equations. To this aim a method based on modern neural network techniques is developed which gives the radial muon wavefunctions as a linear combination of sigmoid functions.

1. Introduction

Recent gauge theories and supersymmetric (SUSY) models going beyond the standard model (SM) allow a great number of lepton-flavour-changing processes [1–5] which can be classified into three categories: the purely leptonic flavour non-conserving processes ($\mu \to e\gamma$, $\mu \to 3e$, $\nu_\mu \to \nu_e$, etc), the meson and hadron decays ($K_L^0 \to \mu^\pm e^\mp$, $K^+ \to \pi^+ e\bar{\mu}$, etc) and the exotic semi-leptonic reactions which take place in the field of nuclei ($\mu^- \to e^-$ or $\mu^- \to e^+$ conversion, etc). Of particular interest are the muon number violating processes due to the fact that the muon is a relatively long-lived particle which can be abundantly produced in muon factories [1, 2]. Among the latter reactions prominent position possesses the neutrinoless capture of a bound 1s muon (μ_b^-) in a muonic atom by the nucleus (A, Z), known as muon–electron conversion,

$$\mu_b^- + (A, Z) \to e^- + (A, Z)^*, \tag{1}$$

(A signifies mass number and Z atomic number of the nucleus). This process violates the conservation of the separate muon (L_μ) and electron (L_e) quantum numbers (lepton flavours) by one unit, but conserves the total lepton (L) quantum number. It has been suggested that process (1) is one of the most sensitive tests of muon number conservation and, recently, there has been intense experimental and theoretical interest to search for this exotic process.

Many experimental attempts to explore process (1) have been performed mainly at PSI on ^{48}Ti, ^{197}Au and ^{208}Pb targets [2, 6–8] and in the earlier years at TRIUMF (on ^{48}Ti and ^{208}Pb) [9]. They yielded branching ratios,

$$R_{\mu e} \equiv \frac{\Gamma(\mu^-, e^-)}{\Gamma(\mu^-, \nu_\mu)} = \frac{\Gamma_{\mu e}(A, Z)}{\Gamma_{\mu c}(A, Z)}, \tag{2}$$

at the level of $R_{\mu e} \leqslant 10^{-13}$–$10^{-12}$. In equation (2) $\Gamma_{\mu e}$ denotes the rate of process (1) and $\Gamma_{\mu c}$ the total rate of the ordinary muon capture [10],

$$\mu_b^- + (A, Z) \rightarrow \nu_\mu + (A, Z-1)^*. \tag{3}$$

The last run of SINDRUM II experiment (PSI) used ^{197}Au as the muon-stopping target and, as has been announced by van der Schaaf recently [7], from the data of this experiment a limit

$$R_{\mu e}^{\mathrm{Au}} \leqslant 5.0 \times 10^{-13},$$

is extracted. This is an improvement over the first limit obtained on ^{197}Au, $R_{\mu e}^{\mathrm{Au}} \leqslant 2.0 \times 10^{-11}$ [8], by a factor of 40 and over the best limit extracted on a heavy target ^{208}Pb, $R_{\mu e}^{\mathrm{Pb}} \leqslant 4.6 \times 10^{-11}$ [6], by about two orders of magnitude. The value of the previous best upper bound was obtained on ^{48}Ti (PSI) at the value $R_{\mu e}^{\mathrm{Ti}} \leqslant 6.1 \times 10^{-13}$ [6].

It should be mentioned that, two future experiments are in preparation for process (1). The planned MECO experiment at Brookhaven National Laboratory (BNL), is going to employ the light target ^{27}Al [11] with the prospect of reaching in the next few years a sensitivity of roughly $R_{\mu e}^{\mathrm{Al}} \leqslant 2 \times 10^{-17}$ [11] which implies an improvement of the present limits by about three orders of magnitude. Very recently, a proposal for another future μ–e conversion experiment (PRIME) in the muon factory at KEK (Japan) was announced [12], in which a ^{48}Ti nucleus will be used as the target with the very high expected sensitivity of $R_{\mu e}^{\mathrm{Ti}} \leqslant 10^{-18}$ [12].

The determination of the rate $\Gamma_{\mu e}$ of equation (2) requires the study of the elementary process $\mu^- + N \rightarrow e^- + N^*$, with $N = p, n$, in some specific particle model and the calculation of nuclear matrix elements involving the nuclear wavefunctions for the initial and final states as well as the muon wavefunction in the 1s atomic orbit [13, 14]. In general, the participation of the nucleus in semi-leptonic processes such as (1), (3) etc constitutes an excellent testing ground not only for highly sophisticated many-body nuclear models but also for theories of fundamental interactions [1, 10]. In the case of the exotic process (1) the relevant theories are extensions of the standard model [15–18], so that nuclear studies of the μ–e conversion can throw light on phenomena connected to new physics. The particle physics aspects of process (1) have comprehensively been studied [3, 19, 20]. The motivation of the present work was the necessity to evaluate accurately the transition matrix elements entering the branching ratio $R_{\mu e}$, i.e. the muon–nucleus overlap integrals, by paying special attention to the precise and convenient calculation of the muon wavefunctions [13]. This, furthermore, offers the possibility of investigating the exact nuclear-structure dependence of $R_{\mu e}$ throughout the periodic table including, of course, the ^{27}Al, ^{48}Ti, ^{197}Au and ^{208}Pb μ–e conversion targets.

Previous estimations of the branching ratio $R_{\mu e}$ [15–17] either treated the bound muon non-relativistically or used the effective nuclear-charge approximation and/or ignored the muon binding energy from the kinematics of process (1). Such calculations were mainly based on the effective evaluation of the muon–nucleus integrals and the use of the quantity Z_{eff} [14], i.e. the effective nuclear charge seen by the muon at the muonic atom. The qualitative variation of $R_{\mu e}$ with atomic number Z resulting in this way shows a maximum around $Z = 29$ [15, 17]. In [18] the solution of the Schrödinger equation was carried out with the Coulomb potential of point-proton densities obtained from the electron scattering data via deconvolution by the nucleon finite size (the neutron densities were obtained from pionic atom data).

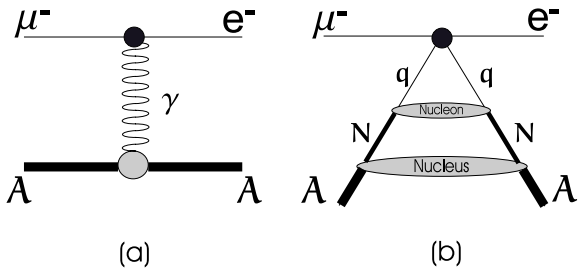

Figure 1. (a) Long-range (photonic) and (b) short-range (non-photonic) mechanisms contributing to the exotic muon–electron conversion in nuclei.

The evaluated ratios $R_{\mu e}$ in [18] saturate around the Pb region (for photonic and non-photonic mechanisms).

Our calculations for $R_{\mu e}$ in the present work are similar to those of [18] but, as we will see, they are more advantageous. We perform direct calculation of the muon–nucleus integrals by first developing a method of solving the Schrödinger and Dirac equations within the framework of neural networks [21]. This method yields the radial components of the muon wavefunctions in the form of analytic expressions given by linear combinations of sigmoid functions (see section 3). For the Coulomb potential we use experimental proton densities, but the use of neural networks avoids the deconvolution needed in [18], so that the finite sizes of the nucleus and nucleon are taken into consideration in a direct way. As we shall see in section 3, the muon binding energy comes out in the minimization procedure of our method. We, moreover, take effectively into account vacuum polarization corrections to the muon binding energy by inserting them into the radial muon wavefunctions [14].

The paper is organized as follows. We first recapitulate the relevant formalism for the branching ratio $R_{\mu e}$ (section 2) and then present the method constructed to solve the Schrödinger and Dirac equations for the radial components of the muon wavefunction (section 3). The obtained results for the branching ratio $R_{\mu e}$ based on the exact muon–nucleus integrals are presented and compared with those given by previous approximations in section 4. The conclusions drawn are summarized in section 5.

2. Formalism for the $\mu^- \to e^-$ conversion branching ratio

In the standard model of the electroweak interactions with massless neutrinos, the lepton-flavour quantum numbers L_i are separately conserved, but in various extensions of the SM lepton-flavour violation (LFV) arises naturally [3, 19]. In general, new particles are required in these models (additional leptons, Higgs particles, scalar SUSY partners of fermions, R-parity violating particles, leptoquarks, etc) [3, 19]. From the non-observation of LFV events in the relevant experiments, upper bounds of such processes can set limits on the masses and couplings of the hypothetical particles involved. On the other hand, the observation, if ever, of some LFV reactions would provide unambiguous evidence for new physics.

In the description of the muon–electron conversion Hamiltonian, two theoretical aspects characterized by different distance scales were distinguished [19, 20]. The long-distance effects related to intermediate virtual photons shown by the diagrams of figure 1(a), and the short-distance effects mediated by other particles involved in the short-range (4-fermion contact interaction) diagrams of figure 1(b). Calculations of the rates for process (1) have been carried out in a variety of particle models [1, 3, 19], but absolute rates are difficult to

predict due to unknown couplings and/or masses of the particles mediating the interactions. The $\mu^- \to e^-$ conversion Hamiltonian which results in the context of such models [19, 20], in general, gives rise to both coherent and incoherent processes leaving the nucleus in the ground state or exciting it, respectively. In several models, e.g. the class for which the isoscalar couplings of the vector and scalar interactions are not very small or zero [5, 19], the coherent contribution of all nucleons in the $\mu^- \to e^-$ leads to enhancement of conversion electrons and, hence, this channel predominates in $R_{\mu e}$ and makes process (1) a sensitive probe for LFV effects.

The experimental signature of reaction (1) is a single mono-energetic electron with energy corresponding to the coherent peak [2], i.e. to the kinematical end point of bound muon decay,

$$E_e^{\rm coh} = E_\mu - m_e - \frac{E_\mu^2}{2M_A}, \tag{4}$$

where $E_\mu = m_\mu - \epsilon_b$, is the muon energy at the 1s state and m_μ (m_e) the muon (electron) mass. ϵ_b denotes the muon binding energy and $E_\mu^2/2M_A$ is the energy of the recoiling nucleus having mass M_A. The branching ratio $R_{\mu e}$ for incoherent processes can be estimated experimentally [6] by taking the difference between the experimental and the Monte Carlo muon decay-in-orbit ($\mu \to e\nu\bar{\nu}$) spectra. Theoretically, the coherent and incoherent channels have been evaluated by state-by-state calculations within quasi-particle random phase approximation (QRPA) [5, 22–24], shell model [25], etc [18]. The calculated incoherent rate, in general, exhausts a small portion (mostly $\leqslant 10\%$) of the total muon conversion rate because the Pauli blocking effects prevent the formation of excited states.

The expression for the branching ratio $R_{\mu e}$, to the leading order of the non-relativistic expansion, for the coherent process has been written in the form [19, 20]

$$R_{\mu e} = \frac{G_F^2}{2\pi}\mathcal{Q}\frac{p_e E_e \left|\mathcal{M}_{V,S}^{(0)}\right|^2}{\Gamma_{\mu c}}. \tag{5}$$

The factor $G_F^2/2$ corresponds to non-photonic mechanisms and for photonic ones it should be replaced by the ratio $(4\pi\alpha)^2/q^4$ where α is the fine structure constant. In equation (5) p_e is the electron momentum connected to the excitation energy E_x of the nucleus through the relation $p_e \approx q = E_e^{\rm coh} - E_x$, where $E_x = E_f - E_{\rm gs}$ is referred to the ground state energy of the daughter nucleus. q denotes the 3-momentum transfer.

In the expression for $R_{\mu e}$, the main nuclear dependence is accounted for by the last fraction of equation (5). The quantity $\mathcal{Q}$ depends very weakly on the nuclear structure and it is roughly determined by the square of scalar (S), vector (V), axial-vector (A), pseudo-scalar (P) and tensor (T) terms of the form

$$\mathcal{Q}_\alpha = \left|\beta_\alpha^0 + \beta_\alpha^1\phi_\alpha\right|^2, \qquad \alpha = S, V, A, P, T, \tag{6}$$

where the parameters β_α^τ include the couplings of the specific particle model (see, e.g., [3, 19, 20]). In reality, the quantities of equation (6) correspond to the Lorentz invariant interaction components and their contributions have usually been investigated separately [3, 19]. The parameters ϕ_α, assuming dominance of the vector or scalar interactions, are defined as

$$\phi_\alpha = \mathcal{M}_\alpha^{(1)}/\mathcal{M}_{V,S}^{(0)}. \tag{7}$$

Evidently, the $\mathcal{Q}$ of equation (5) depends on the nuclear structure through the factors ϕ_α of equation (7) which are generally small [19, 20]. For photonic diagrams $\phi_V = 1$ (see equation (13)), meaning that Q is rather nuclear structure independent. We note that, the (A, Z) dependence of β_α^τ, which are mainly smooth functions of the momentum transfer

q [3, 19], is not significant, since the variation of q from light to heavy nuclei is of the order of ϵ_b.

In the general case, the matrix elements $\mathcal{M}_\alpha^{(\tau)}$ entering the expression of $R_{\mu e}$ assuming non-relativistic muons are written as

$$\mathcal{M}_\alpha^{(\tau)} = \langle f| \sum_{j=1}^{A} \Theta_\alpha^\tau(j)\, \mathrm{e}^{-\mathrm{i}\mathbf{q}\cdot\mathbf{r}_j}\, \Phi(\mathbf{r}_j)|i\rangle, \tag{8}$$

where $|i\rangle$ represents the initial and $|f\rangle$ the final state of the daughter nucleus. $\Phi_\mu(\mathbf{r}_j)$ represents the radial part of the large (top) component of the muon spinor at the position of the jth target-nucleon. The functions $\Theta_\alpha^\tau(j)$ contain the spin–isospin dependence of the $\mu^- \to e^-$ operator and (ignoring the small tensor term) they take the form

$$\Theta_\alpha^\tau(j) = \begin{cases} \theta^\tau(j), & \text{for} \quad \alpha = S, V \\ \theta^\tau(j)\boldsymbol{\sigma}/\sqrt{3}, & \text{for} \quad \alpha = A \\ \theta^\tau(j)\hat{\mathbf{q}}\cdot\boldsymbol{\sigma}/\sqrt{3}, & \text{for} \quad \alpha = P \end{cases} \tag{9}$$

where $\theta^0(j) = 1, \theta^1(j) = \tau_{3j}$ and $\hat{\mathbf{q}}$ is the unit vector in the direction of the momentum transfer.

The methods of evaluating the $\mathcal{M}_\alpha^{(\tau)}(q)$ can be classified into two types according to how they treat the integrals of equation (8). The first determines them numerically using an exact muon wavefunction and the second uses an effective calculation of these integrals.

(1) For the coherent process ($|f\rangle = |i\rangle$), in the case of scalar and vector interactions, $\mathcal{M}_\alpha^{(\tau)}$ are written in terms of the ground-state proton and neutron densities ρ_p and ρ_n as

$$\mathcal{M}_{V,S}^{(\tau)} = \int [\rho_p(\mathbf{r}) \pm \rho_n(\mathbf{r})]\, \mathrm{e}^{-\mathrm{i}\mathbf{q}\cdot\mathbf{r}} \Phi_\mu(\mathbf{r})\, \mathrm{d}^3\mathbf{r} \equiv \mathcal{F}_p \pm \mathcal{F}_n, \tag{10}$$

$$\mathcal{F}_{p,n}(\mathbf{q}) = \int \rho_{p,n}(\mathbf{r})\, \mathrm{e}^{-\mathrm{i}\mathbf{q}\cdot\mathbf{r}} \Phi_\mu(\mathbf{r})\, \mathrm{d}^3\mathbf{r} \tag{11}$$

(the (+) sign corresponds to the isoscalar $\tau = 0$ and the (−) to the isovector $\tau = 1$ channel). The proton (neutron) density ρ_p (ρ_n) is normalized to the atomic (neutron) number $Z(N)$ of the participating nucleus in process (1). For spherically symmetric nuclei, the following integral representation for $\mathcal{F}_{p,n}$ is valid

$$\mathcal{F}_{p,n}(q) = 4\pi \int j_0(qr)\Phi_\mu(r)\rho_{p,n}(r) r^2\, \mathrm{d}r, \tag{12}$$

where $j_0(x)$ represents the zero-order spherical Bessel function. In photon-exchange mechanisms (only the protons of the target nucleons participate) for the g.s. $\to$ g.s. transition the following relation holds:

$$\mathcal{M}_V^{(0)} = \mathcal{M}_V^{(1)} = \mathcal{F}_p(q). \tag{13}$$

(2) For light and medium nuclei, the matrix elements $\mathcal{M}_\alpha^{(\tau)}$ can be approximated by factorizing outside the integrals of equation (8) a suitable average muon wavefunction $\langle\Phi_\mu^{1s}\rangle$ as

$$\overline{\mathcal{M}}_\alpha^{(\tau)} = \langle\Phi_\mu^{1s}\rangle \langle f| \sum_{j=1}^{A} \Theta_\alpha^\tau(j)\, \mathrm{e}^{-\mathrm{i}\mathbf{q}\cdot\mathbf{r}_j}|i\rangle \equiv \langle\Phi_\mu^{1s}\rangle M_\alpha^{(\tau)}, \tag{14}$$

where $M_\alpha^{(\tau)}$ accumulate the pure nuclear physics aspects of the $\mu^- \to e^-$ conversion rates. In the allowed muon capture process an approximation for the average value of $\langle\Phi_\mu^{1s}(r)\rangle$ was used by many authors [1, 10, 26]. It is given in terms of the effective charge Z_{eff} as

$$\langle\Phi_\mu^{1s}\rangle^2 = \frac{\int |\Phi_\mu(\mathbf{r})|^2 \rho(\mathbf{r})\, \mathrm{d}^3\mathbf{r}}{\int \rho(\mathbf{r})\, \mathrm{d}^3\mathbf{r}} = \frac{\alpha^3 m_\mu^3}{\pi} \frac{Z_{\mathrm{eff}}^4}{Z}. \tag{15}$$

In previous estimations of the branching ratio $R_{\mu e}$ [3, 17], the same expression for $\langle \Phi_\mu^{1s} \rangle$ was adopted for both the numerator and the denominator of equation (2) in order to reduce as much as possible the uncertainties that appeared for heavy nuclear systems.

For g.s. $\rightarrow$ g.s. transitions, the nuclear matrix elements $M_{V,S}^{(\tau)}$ in equation (14) are determined from the elastic scattering nuclear form factors F_p, F_n [17, 29] as

$$M_{V,S}^{(\tau)} = ZF_p(q) \pm NF_n(q) \tag{16}$$

(the correspondence of signs is as in equation (10)). For photonic mechanisms the latter expression leads to $M_V^{(0)} = M_V^{(1)} = ZF_p(q)$. In the case of nuclei with spin $J_{\rm gs} \neq 0$ in the ground state (e.g. ^{27}Al, the MECO target, has $J_{\rm gs} = \frac{5}{2}$ and ^{197}Au, the SINDRUM II target, has $J_{\rm gs} = \frac{3}{2}$), the exact $F_{p,n}$ contain additional contributions from other multipoles as [30]

$$|F_T(q)|^2 = \frac{4\pi}{T^2} \frac{1}{2J_{\rm gs}+1} \sum_{L=\text{even}} |\langle J_{\rm gs}||\hat{M}_L(qr)||J_{\rm gs}\rangle|^2 \tag{17}$$

$$\hat{M}_L(qr) = \sum_{i=1}^{A} \frac{1 \pm \tau_{3i}}{2} j_L(p_e r_i) Y_L^M(\hat{r}_i) \delta(\mathbf{r} - \mathbf{r}_i) \tag{18}$$

(the (+) sign and $T = Z$ corresponds to protons while the (−) sign and $T = N$ to neutrons). This means that, in general, in addition to the monopole ($L = 0$) elastic scattering nuclear form factor, the contribution arising from other (even) multipoles ($L = 2, 4, \ldots$) must be calculated. For spin-0 light nuclei ($J_{\rm gs} = 0$ and only $L = 0$ contributes) equation (17) gives

$$F_T(q) = \frac{4\pi}{T} \int j_0(p_e r) \rho_T(r) r^2 \, \mathrm{d}r. \tag{19}$$

Note that, in the case when $F_Z \approx F_N \approx F_A$ (for vector and scalar interactions) by substituting equation (14) into equation (7) we obtain (see [16])

$$\phi_{S,V} \approx (A - 2Z)/A, \tag{20}$$

an approximation which is reasonable only for light nuclear systems.

In the present work, we calculate the integrals of equation (8) explicitly by first obtaining the muon wavefunction $\Phi_\mu(r)$ from the solution of Schrödinger (or Dirac) equation using the method described in the following section.

3. The muon wavefunctions with neural networks

It is well known that, in the approximation of a point-like nucleus the hydrogenic-type muon wavefunction is readily obtained, since in this case the Schrödinger and Dirac equations can be solved analytically. Assuming the finite sizes for the nucleus and nucleon, one must solve these equations numerically. We now exploit the advantages of the neural networks to obtain analytic expressions for the radial part of the muon wavefunctions in both cases.

3.1. Solution of the Schrödinger equation for the muon

As mentioned in the introduction, in several approaches the nuclear level μ–e conversion formalism relies on non-relativistic muons. This is equivalent to using only the large component of the muon spinor (the small one is assumed to be zero). In such cases, one solves the Schrödinger equation which for the reduced radial muon wavefunction $u(r) = r\Phi_\mu(r)$ is written as

$$-\frac{\hbar^2}{2m} \frac{\mathrm{d}^2}{\mathrm{d}r^2} u(r) + V(r)u(r) = Eu(r). \tag{21}$$

$u(r)$ obeys the boundary condition $u\,(r=0)=0$ with asymptotic behaviour $u(r)\sim \mathrm{e}^{-kr}$. In equation (21) m is the reduced muon mass given by

$$\frac{1}{m}=\frac{1}{m_\mu}+\frac{1}{Zm_p+(A-Z)m_n},$$

with m_p (m_n) standing for the proton (neutron) mass. Obviously, for a point-like nucleus, the potential $V(r)$ originates mainly from the Coulomb field of the point-nucleon charge distribution $\rho(\mathbf{r})$ and equation (21) is solved trivially. However, by taking into consideration the finite sizes of the nucleus and nucleons, $V(r)$ needs numerical integration as

$$V(\mathbf{r})=-\mathrm{e}^2\int_0^\infty \frac{\rho(\mathbf{r}')}{|\mathbf{r}-\mathbf{r}'|}\,\mathrm{d}^3r'. \tag{22}$$

By multiplying equation (21) by $u(r)$ and integrating, for spherically symmetric nuclei we obtain

$$-\frac{\hbar^2}{2m}\int u(r)\frac{\mathrm{d}^2}{\mathrm{d}r^2}u(r)\,\mathrm{d}r+\int V(r)u(r)^2\,\mathrm{d}r=E\int u(r)^2\,\mathrm{d}r. \tag{23}$$

Integrating the term with the second derivative by parts and solving for the energy E we find

$$E=N_0\frac{\hbar^2}{2m}\int\left[\frac{\mathrm{d}u(r)}{\mathrm{d}r}^2+V(r)u(r)^2\right]\mathrm{d}r, \tag{24}$$

where N_0 is the normalization factor

$$N_0=\left[\int u(r)^2\,\mathrm{d}r\right]^{-1}.$$

If we construct a grid from $r=0$ up to a point $r=b$ where the wavefunction is practically vanishing (see below), and denote it by r_i, for $i=1,2,\ldots,n$, then equation (21) must hold at every point r_i of the grid. This is equivalently expressed as

$$\sum_{i=1}^{n}\left[-\frac{\hbar^2}{2m}\frac{\mathrm{d}^2}{\mathrm{d}r^2}u(r_i)+V(r_i)u(r_i)-Eu(r_i)\right]^2=0. \tag{25}$$

Our approach to solve the latter equation consists in parametrizing $u(r)$ and then minimizing the left-hand side of equation (25) divided by the normalization $\int u(r)^2\,\mathrm{d}r$, so as to avoid the trivial solution $u(r)=0$ everywhere. To this aim we use the parametrization

$$u(r)=r\,\mathrm{e}^{-kr}N(r,\vec{u},\vec{w},\vec{v}),\qquad k>0, \tag{26}$$

where $N(r,\vec{u},\vec{w},\vec{v})$ is a feed-forward artificial neural network with one hidden layer and one input unit (r) (for details see [21]). The biases are denoted by $\vec{u}=(u_1,u_2,\ldots,u_m)$ where m is the number of hidden units. The weights to the hidden layers are denoted by $\vec{w}=(w_1,w_2,\ldots,w_m)$ and the weights to the output by $\vec{v}=(v_1,v_2,\ldots,v_m)$. The hidden layer units have sigmoid activations of the form $f(x)=(1+\mathrm{e}^{-x})^{-1}$. Specifically we have

$$N(r,\vec{u},\vec{w},\vec{v})=\sum_{i=1}^{m}v_i\,f(w_ir+u_i). \tag{27}$$

To obtain the precise expression for the reduced radial wavefunction $u(r)$, we insert this form in equation (26). We then train the network so as to minimize the left-hand side of equation (25) down to a quantity close enough to zero for all practical purposes, by adjusting the biases (u_i) and weights (w_i). The muon binding energy ϵ_b in the 1s atomic orbit is determined from the minimum energy, $E_{\min}=\epsilon_b$, satisfying equation (25). The training in our method is performed by the Merlin/MCL software package [27], that proved to be both convenient and efficient.

3.2. Solution of the Dirac equation for the muon

The confidence level of using non-relativistic muon wavefunctions in $\mu^- \to e^-$ conversion calculations can to a large extent be estimated by solving in addition to Schrödinger the Dirac equation and obtaining the small component of the muon spinor as well. This is a Dirac-equation-based relativistic approach for the $\mu^- \to e^-$ reaction. In our method, the Dirac equation is solved in a similar but a bit more involved manner to that discussed in the previous subsection (for details the reader is referred to [21]).

It should be noted that, for both the Schrödinger and Dirac solutions one has to take into account some may be significant corrections to the potential of equation (21) such as the nuclear polarization [13], the vacuum polarization [14], etc. In the present work, we have considered the vacuum polarization corrections described by an effective potential as in [14]. It must also be mentioned that, for large distances the matching of the wavefunctions to their asymptotic behaviour was done as in [21]. For light nuclei this matching was done at $r = b \approx 60$–70 fm and for heavy isotopes at $r = b \approx 40$ fm.

Before closing this section it is worth making the following remarks: the advantages of utilizing equations (26)–(27) for the muon wavefunctions become more evident when one calculates the incoherent rate of a muonic process ($\mu^- \to e^-$, $\mu^- \to e^+$ etc), where one has to face a large number of (double or multiple) numerical integrations corresponding to the final states included in a chosen model space. In addition, due to the fact that in our method the muon wavefunctions are available in a convenient way, i.e. as linear combinations of well-behaved (sigmoid) functions, the use of extrapolation and/or interpolation techniques required in other methods [16–18] is avoided and the accuracy of the results obtained this way is very high. In our present calculations, the accuracy has been checked by evaluating the ground-state energy (i.e. the muon binding energy at the 1s atomic orbit) in the case of exact analytical solutions of the Schrödinger equation (assuming point-like nuclear densities) for some representative nuclear isotopes. We found that, the results of our method are in excellent agreement with the exact analytical results (the differences are of the order of 10^{-8}–10^{-7}).

4. Results and discussion

The above formalism has been applied in the present work to study the exact dependence of the branching ratio $R_{\mu e}(A, Z)$ on the parameters A and Z for a series of nuclear isotopes including those which are of current experimental interest (the light ^{27}Al, ^{48}Ti and the heavy ^{197}Au, ^{208}Pb muon-stopping targets). The integrals of equation (10) have been computed by utilizing the precise muon wavefunctions of equations (26)–(27). To this aim, we parametrized the trial muon wavefunctions, $\Phi_\mu(r)$ for the Schrödinger equation and $f_\mu(r)$ (large component) and $g_\mu(r)$ (small component) for the Dirac equation, as described in section 3. In equation (27) we have chosen $m = 5$ sigmoid hidden units even though smaller values of m, e.g. $m = 3$, give only slightly different results (for Dirac solutions using $m = 3$ the resulting modification is less than 1%). Thus, the total number of parameters used for the present calculations is typically 15, but some of them are practically zero ($\leqslant 10^{-5}$). We have considered 100 equidistant points in the range $[r = 0, r = b]$, where b is the parameter matching the muon wavefunctions to their asymptotic behaviour (see section 3.2). The required integrations have been performed by using the Gauss–Legendre rule.

In this paper, we restrict ourselves to the photonic mechanism where only the target protons contribute to $R_{\mu e}$ and ϕ_V of equation (7) becomes equal to unity. We focus on the investigation of the following effects on the results for $R_{\mu e}$: (i) The consideration of the outgoing muon in $\mu^- \to e^-$ as a relativistic particle which is estimated by comparing the radial

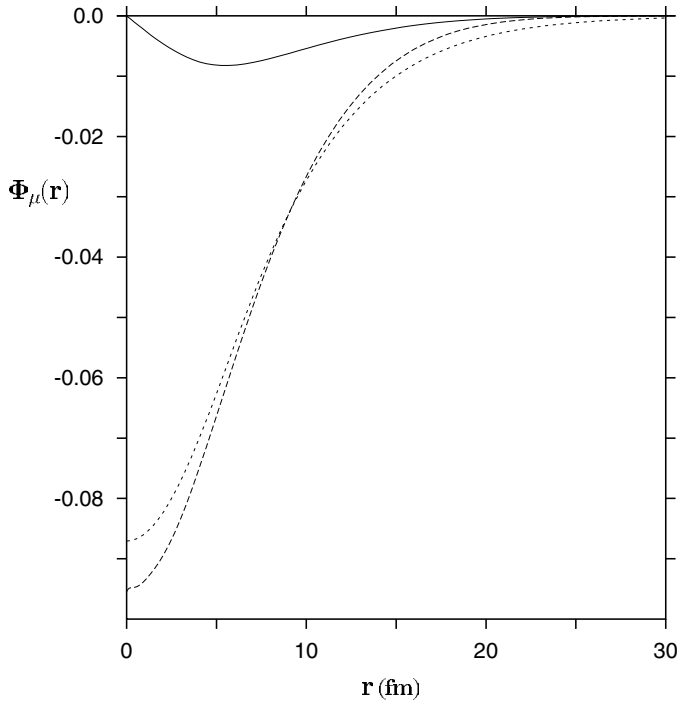

Figure 2. Dirac spinor for a muon bound in ^{208}Pb: The large (top) component (dashed line) and the small (bottom) component (solid line). For comparison the corresponding Schrödinger solution (long-dashed line) is also shown.

Dirac wavefunctions for the muon with the Schrödinger one. (ii) The neglect of the muon binding energy ϵ_b in equation (4), an assumption which implies that, in the coherent mode the momentum and energy transfers to any nucleus are approximately given by

$$q \approx p_e \approx m_\mu/c = 0.534\ \text{fm}^{-1}, \qquad E_e \approx m_\mu c^2 = 105.6\ \text{MeV}. \tag{28}$$

(iii) The use of expression (14) for an approximate evaluation of the muon–nucleus integrals of equation (8).

The first effect is illustrated in figure 2 where the two components of the radial Dirac (1s) wavefunction for a muon trapped in the heavy ^{208}Pb isotope are plotted (solid line corresponds to the small component and short-dashed line to the large one) and compared with the Schrödinger wavefunction (long-dashed line). We note that, the effect of treating the muon relativistically is more pronounced in heavy nuclei compared to that in light ones. As can be seen from figure 2, the values of the small Dirac component in the region of $r \leqslant 7$ fm (where the density of ^{208}Pb takes appreciable values) are always smaller than the 10–15% of the corresponding values of the large component. Furthermore, the large (top) component of the Dirac spinor does not significantly differ from the Schrödinger wavefunction (the differences are of the order of 10%).

In table 1 we quote the ingredients needed to evaluate $R_{\mu e}$ for the case of assuming an average muon wavefunction. The proton form factors are computed from the electron scattering data of [29] at the values of momentum transfer given: (a) by equation (28) when ϵ_b is ignored (fifth column) and (b) by equation (4) when ϵ_b is taken into account (last column).

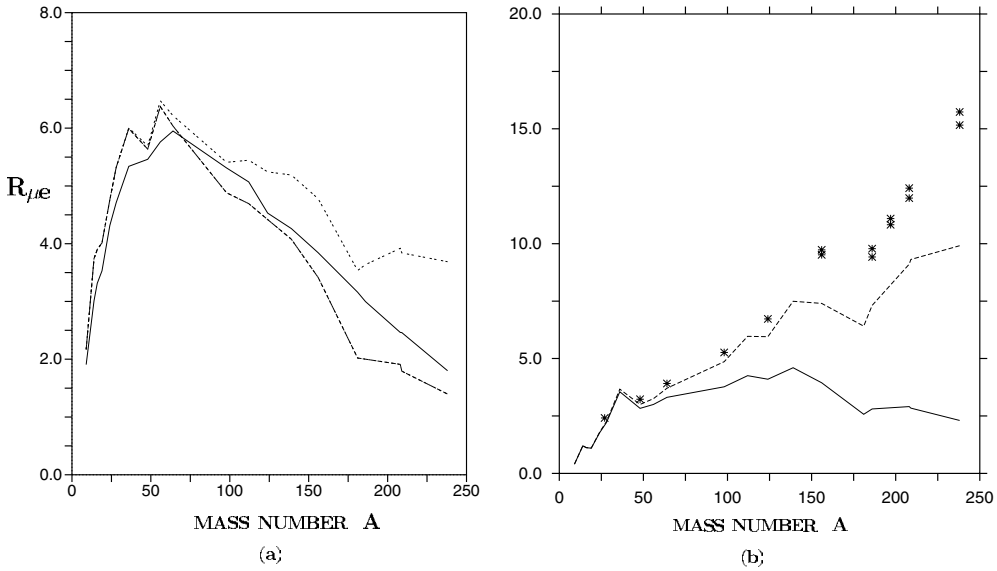

Figure 3. Variation of the $\mu^- \to e^-$ conversion branching ratio $R_{\mu e}(A, Z)$ throughout the periodic table: For the curves in (a) the phenomenological formula of [15], equation (29), in various cases was employed and for the curves in (b) the results of $\langle R_{\mu e}\rangle/\mathcal{Q}_{ph}$ of equation (30) and those of $R_{\mu e}/\mathcal{Q}_{ph}$ of equation (31) are plotted. For details see the text.

Table 1. Elastic scattering nuclear form factors [29] $F_p(q)$ at $q = m_\mu = 0.535$ fm^{-1} and at $q = p_e = m_\mu - \epsilon_b$, with ϵ_b the muon binding energy in the specific muonic atom.

A	Z	ϵ_b (MeV)	p_e(fm^{-1})	$F_p(m_\mu)$	$F_p(p_e)$
24	12	0.38	0.533	0.630	0.632
28	14	0.54	0.532	0.617	0.620
48	22	1.25	0.529	0.506	0.515
64	30	2.21	0.524	0.449	0.465
98	42	3.94	0.515	0.341	0.373
124	50	5.20	0.509	0.297	0.341
156	64	6.33	0.497	0.231	0.294
186	74	9.10	0.489	0.165	0.243
208	82	10.59	0.482	0.153	0.243
238	92	12.16	0.474	0.123	0.226

The results of $R_{\mu e}$ in various approximations and the main steps followed for our calculations are discussed below.

(1) At first the variation of the quantity $Z|F_Z(q)|^2$ through the periodic table is studied. As is known, in [15] it was wrongly concluded that for the coherent $\mu^- \to e^-$ branching ratio the following relation holds:

$$R_{\mu e} \propto Z|F_{NN}(q)|^2. \tag{29}$$

The empirical expression for F_{NN} is given in [15]. In figure 3(a) we plot the results obtained with equation (29) for the following cases.

Table 2. Matrix elements of equation (14) calculated with mean muon wavefunctions. The values of the ratio $\langle R_{\mu e}\rangle/\mathcal{Q}_{ph}$ of equation (30) are also quoted.

A	Z	$\langle\Phi_\mu\rangle ZF_p(m_\mu)$ (fm$^{-3/2}$)	$\langle\Phi_\mu\rangle ZF_p(p_e)$ (fm$^{-3/2}$)	$\langle R_{\mu e}(m_\mu)\rangle/\mathcal{Q}_{ph}$	$\langle R_{\mu e}(p_e)\rangle/\mathcal{Q}_{ph}$
16	8	0.015	0.015	1.118	1.124
19	9	0.019	0.019	1.097	1.105
24	12	0.034	0.034	1.776	1.802
28	14	0.047	0.048	2.211	2.256
36	18	0.075	0.075	3.555	3.668
48	22	0.099	0.100	2.831	2.999
56	26	0.133	0.137	3.001	3.253
64	30	0.158	0.164	3.310	3.708
98	42	0.212	0.231	3.769	4.861
112	48	0.237	0.268	4.255	5.968
124	50	0.237	0.272	4.098	5.953
139	57	0.254	0.305	4.598	7.493
156	64	0.250	0.318	3.947	7.402
181	73	0.208	0.301	2.573	6.412
186	74	0.209	0.309	2.805	7.314
208	82	0.222	0.354	2.908	9.108
209	83	0.213	0.347	2.844	9.316
238	92	0.199	0.365	2.303	9.911

(i) The experimental form factors [29] are inserted in equation (29), $F_{NN}(q) \equiv F_Z(q)$, at the values of q given: (a) by equation (28) (dashed-dotted line) and (b) by equation (4) (dotted line).

(ii) The phenomenological expression for $F_{NN}(q)$ (see equation (16) of [15]) is plugged in equation (29) (solid line).

As can be seen from figure 3(a), the three curves of cases (i) and (ii) show maximum branching ratio in the region of $A \approx 60$ (copper region) as had been estimated in [15] and verified (under the same assumptions) using shell model nuclear form factors in [17]. This feature was previously adopted by some experimentalists exploring the $\mu^- \to e^-$ process [9]. We also see from figure 3(a) that, in the region of light nuclei the three curves nearly coincide, which indicates that the approximation of equation (28) is reasonable in that region, but for medium and heavy nuclei where ϵ_b becomes significant, the resulting rates with the exact q (given by equation (4)) are sometimes larger by a factor of about 2 compared to those obtained when ϵ_b is ignored in the kinematics of $\mu^- \to e^-$.

(2) The second part of our calculations deals with the variation of the ratio $R_{\mu e}/\mathcal{Q}_{ph}$ (see equation (5)) which accumulates the main nuclear-structure dependence of $R_{\mu e}$. Two cases are distinguished.

(i) The average muon wavefunction of equation (15) is inserted in equation (5). This gives

$$\frac{\langle R_{\mu e}\rangle}{\mathcal{Q}_{ph}} = 16\pi\alpha^2 \frac{p_e E_e}{q^4} \frac{\langle\Phi_\mu\rangle^2 Z^2 |F_p(q)|^2}{\Gamma_{\mu c}}. \tag{30}$$

In table 2 we present the results obtained in a set of nuclei for the matrix elements $\overline{\mathcal{M}}$ of equation (14) and for the ratio $\langle R_{\mu e}\rangle/\mathcal{Q}_{ph}$ of equation (30). These results rely on the use of the average muon wavefunction and correspond to the two choices (a) and (b) of the momentum transfer discussed before. For comparison, the results of $\langle R_{\mu e}\rangle/\mathcal{Q}_{ph}$ are,

Table 3. Exact calculation of the parameter $\mathcal{F}_p$ of equation (11) and of the ratio $R_{\mu e}/\mathcal{Q}_{ph}$ of equation (31). The experimental muon capture rates [28] are also quoted.

A	Z	$\Gamma_{\mu c}(\times 10^6)$ (s^{-1})	$\lvert\mathcal{F}_p\rvert$($fm^{-3/2}$)	$R_{\mu e}/\mathcal{Q}_{ph}$
27	13	0.71	0.047	2.412
48	22	2.63	0.104	3.228
64	30	5.76	0.168	3.916
98	42	9.07	0.241	5.266
124	50	10.50	0.289	6.725
156	64	12.09	0.361	9.513
156	64	11.82	0.361	9.730
186	74	11.90	0.357	9.784
186	74	12.36	0.357	9.420
197	79	13.39	0.395	10.826
197	79	13.07	0.395	11.091
208	82	12.98	0.414	12.420
208	82	13.45	0.414	11.986
238	92	12.62	0.451	15.737
238	92	13.10	0.451	15.160

furthermore, plotted in figure 3(b). From the results of choice (a) (solid line) we conclude that $R_{\mu e}(A, Z)$ presents a maximum at the region of $A \approx 130$ which is not in accordance with the estimation of [15]. This is due to the fact that in [15] the theoretical expression for the gross nuclear dependence of $\Gamma_{\mu c}$ was considered as linear in Z, that is equivalent to a constant Primakoff function $f_{GP}(A, Z)$ [26]. It is well known, however, that $\Gamma_{\mu c}$ is rather strongly dependent on the mass excess [26] (see also erratum of [15]). In the present work, in order to minimize such uncertainties, we used the experimental data for the total muon capture rates $\Gamma_{\mu c}$ [28]. From the results of choice (b) (dashed line), one can conclude that $R_{\mu e}(A, Z)$ shows a slow increase up to the heaviest nuclei.

(ii) Finally, for the investigation of $R_{\mu e}(A, Z)$ the exact muon–nucleus integrals of equation (10) are inserted in equation (5). The precise muon wavefunctions are calculated for each isotope as is described in section 3. In table 3 we list the results of $\mathcal{F}_p$ defined in equation (11) and those of the ratio

$$\frac{R_{\mu e}}{\mathcal{Q}_{ph}} = 16\pi\alpha^2 \frac{p_e E_e}{q^4} \frac{|\mathcal{F}_p|^2}{\Gamma_{\mu c}}, \tag{31}$$

both evaluated at the exact momentum transfer q provided by equation (4). We again used experimental muon capture rates (see table 3) and for some heavy isotopes we employed two different values of $\Gamma_{\mu c}$ (they correspond to the smallest and largest measurement quoted in [28]). For heavy nuclei the experimental muon capture data exhibit larger uncertainties compared to those for light ones.

The nuclear variation of $R_{\mu e}(A, Z)$ arising from the results of table 3 (points represented by asterisks (∗)) is illustrated in figure 3(b). We note that, on the basis of the exact evaluation of the muon–nucleus integrals throughout the periodic table, $R_{\mu e}$ keeps increasing as a function of A (or Z) up to the heaviest isotopes. For heavy and very heavy nuclei (region of ^{197}Au and ^{208}Pb) equation (31) gives much larger rates than the approximation of the averaged muon wavefunction equation (30). The comparison is much worse if ϵ_b is neglected in the kinematics of $\mu^- \to e^-$. One must note that, in the case when q is given by equation (4), the factor q^{-4}

in equation (31) inserts in the branching ratio $R_{\mu e}$ an additional (A, Z) dependence that had previously been overlooked [15–18]. Thus, the crude overall picture of the behaviour of $R_{\mu e}$ obtained by the exact muon–nucleus integrals, exhibits roughly a linear rise with A (or Z) which can be attributed to the coherent effect. This implies that very heavy nuclei are favoured to be used as $\mu^- \to e^-$ conversion targets unless the existing difference in the branching ratio $R_{\mu e}$ (which in the range of $27 \leqslant A \leqslant 238$ could sometimes become even a factor of about 4) can be compensated by other experimental advantages of specific muon-stopping targets [2, 9]. This conclusion of our results is in qualitative agreement with the variation of $R_{\mu e}$ described in [18].

Before closing, it is worth making the following remarks: (i) Our theoretical results refer to pure isotopes while the relevant experiments use natural (non-enriched) targets [2]. (ii) In the present work the distortion of the Coulomb field by the emitted electron has not been explicitly taken into account. In the literature, the consideration of Coulomb corrections to the wavefunctions of charged leptons participating in various semi-leptonic processes is done by many methods [31–33]. For the $\mu^- \to e^-$ conversion, the estimated modification of the branching ratio $R_{\mu e}$ due to the change of the Coulomb field by the outgoing e^- is not very important (at least for the electron S and P waves assumed in our calculations) [31]. In some other methods, however, the total effect appears to be significant in the region of heavy nuclei [32]. A systematic study of this effect is going to be discussed in connection with other similar processes elsewhere [33]. (iii) The Dirac-equation-based relativistic effects estimated here, are not very significant. However, some other atomic relativistic effects may produce more important components to the muon wavefunction in heavy muonic atoms, which, in particular when non-photonic mechanisms (not discussed here) prevail, may alter a bit the results for $R_{\mu e}$ [33]. We should mention that, recently, the atomic physics aspects of the muon wavefunction have comprehensively been addressed [13] and a method for calculating such corrections to the muonic energy levels has been developed which is applicable only for light muonic atoms [13].

5. Summary and conclusions

One of the main concerns in the present work, was the discussion of the current theoretical background of the muon number non-conserving $\mu^- \to e^-$ conversion. This semi-leptonic exotic process is an interesting and important one to be studied since stringent bounds already exist and significant improvements over these limits are feasible in the near future (SINDRUM II, MECO, PRIME experiments). The new ideas for muon beam intensity and background suppression in $\mu^- \to e^-$ searches might permit stringent tests of many particle models. Moreover, the muon–electron conversion is one of the most promising reactions to look for new physics since it offers more powerful constraints for the charged-lepton flavour violation parameter-space compared to other muon number non-conserving leptonic processes such as $\mu \to e\gamma$, $\mu \to 3e$, etc.

We have extensively investigated the $\mu^- \to e^-$ conversion rates $R_{\mu e}(A, Z)$ (throughout the periodic table) by developing a method for direct calculation of the muon–nucleus integrals entering $R_{\mu e}$. This method uses the precise muon wavefunctions obtained by employing neural network techniques in the form of a sum over few sigmoid functions. We have, furthermore, exploited these muon wavefunctions, both in the Schrödinger and Dirac pictures, to test some approximations used in the past for searching the $\mu^- \to e^-$ conversion and other similar processes. Our results for the photonic mechanism show that $R_{\mu e}(A, Z)$ keeps increasing with A indicating that the very heavy isotopes (Au, Pb, etc) are from that point of view favoured to be used as targets in $\mu^- \to e^-$ experiments.

References

[1] Scheck P 1979 *Phys. Rep.* **44** 187
[2] van der Schaaf A 1993 *Prog. Part. Nucl. Phys.* **31** 1
[3] Kosmas T S, Leontaris G K and Vergados J D 1994 *Prog. Part. Nucl. Phys.* **33** 397
[4] Kosmas T S, Faessler A and Vergados J D 1997 *J. Phys. G: Nucl. Part. Phys.* **23** 693
[5] Kosmas T S 2001 *Nucl. Phys.* A **683** 443
[6] Dohmen C *et al* (SINDRUM II Collaboration) 1993 *Phys. Lett.* B **317** 631
Honecker W *et al* 1996 *Phys. Rev. Lett.* **76** 200
[7] van der Schaaf A (SINDRUM II Collaboration) 2001 Invited talk at *3rd Int. Workshop on Neutrino Factories based on Muon Storage Rings NuFACT'01 (Tsukuba, Japan, 24–30 May 2001)*
[8] Wintz P 2000 Status of muon to electron conversion at PSI Invited talk at *Workshop on New Initiatives in LFV and Neutrino Oscillations with Very Intense Muon and Neutrino Beams (Honolulu-Hawaii, USA, 2–6 Oct. 2000)*
[9] Ahmad S *et al* (TRIUMF Collaboration) 1987 *Phys. Rev. Lett.* **59** 970
[10] Rosenfelder R 1977 *Nucl. Phys.* A **290** 315
Rosenfelder R 1978 *Nucl. Phys.* A **298** 397
[11] Sculli J 2000 The MECO experiment Invited talk at *Workshop on New Initiatives in LFV and Neutrino Oscillations with Very Intense Muon and Neutrino Beams (Honolulu-Hawaii, USA, 2–6 Oct. 2000)*
[12] Kuno Y 2000 The PRISM: beam-experiments Invited talk at *Workshop on New Initiatives in LFV and Neutrino Oscillations with Very Intense Muon and Neutrino Beams (Honolulu-Hawaii, USA, 2–6 Oct. 2000)*
Aoki M 2001 The PRIME experiment Invited talk at *3rd Int. Workshop on Neutrino Factories based on Muon Storage Rings NuFACT'01 (Tsukuba, Japan, 24–30 May 2001)*
[13] Rosenfelder R 1983 *Nucl. Phys.* A **393** 301
Rosenfelder R 1999 *Phys. Lett.* B **463** 317
Lu Y and Rosenfelder R 1993 *Phys. Lett.* B **319** 7
[14] Sens J C 1959 *Phys. Rev.* **113** 679
Ford K W and Wills J G 1962 *Nucl. Phys.* **35** 295
[15] Weinberg S and Feinberg G 1959 *Phys. Rev. Lett.* **3** 111
Weinberg S and Feinberg G 1959 *Phys. Rev. Lett.* **3** 244 (erratum)
[16] Ernst F J 1960 *Phys. Rev. Lett.* **5** 478
Marciano W J and Sanda A I 1977 *Phys. Rev. Lett.* **38** 1512
Shanker O 1979 *Phys. Rev.* D **20** 1608
[17] Kosmas T S and Vergados J D 1988 *Phys. Lett.* B **215** 460
[18] Chiang H C, Oset E, Kosmas T S, Faessler A and Vergados J D 1993 *Nucl. Phys.* A **559** 526
[19] Faessler A, Kosmas T S, Kovalenko S and Vergados J D 2000 *Nucl. Phys.* B **587** 25
Kosmas T S and Kovalenko S 2000 *Phys. At. Nucl.* **63** 1200
[20] Kosmas T S, Kovalenko S and Schmidt I 2001 *Phys. Lett.* B **511** 203
Kosmas T S, Kovalenko S and Schmidt I 2001 *Phys. Lett.* B **519** 78
[21] Lagaris I E, Likas A and Fotiadis D 1997 *Comput. Phys. Commun.* **103** 112
Lagaris I E, Likas A and Fotiadis D 1997 *Comput. Phys. Commun.* **104** 1
[22] Kosmas T S, Vergados J D, Civitarese O and Faessler A 1994 *Nucl. Phys.* A **570** 637
[23] Schwieger J, Kosmas T S and Faessler A 1998 *Phys. Lett.* B **443** 7
[24] Kosmas T S, Ren Z and Faessler A 2000 *Nucl. Phys.* A **665** 183
[25] Siiskonen T, Suhonen J and Kosmas T S 1999 *Phys. Rev.* C **60** R62501
Siiskonen T, Suhonen J and Kosmas T S 2000 *Phys. Rev.* C **62** 035502
[26] Goulard B and Primakoff H 1974 *Phys. Rev.* C **10** 2034
Hänscheid H *et al* 1990 *Z. Phys.* A **335** 1
[27] Papageorgiou D G, Demetropoulos I N and Lagaris I E 1998 *Comput. Phys. Commun.* **109** 227
Papageorgiou D G, Demetropoulos I N and Lagaris I E 1998 *Comput. Phys. Commun.* **109** 250
[28] Suzuki T, Mearsday D and Roalsvig J 1987 *Phys. Rev.* C **35** 236
[29] de Vries H, de Jager C W and de Vries C 1987 *At. Data Nucl. Data Tables* **36** 495
[30] Donnelly T W and Walecka J D 1975 *Annu. Rev. Nucl. Sci.* **25** 329
[31] Doi M, Kotani T and Takasugi E 1985 *Prog. Theor. Phys. Suppl.* **83** 1
[32] Simkovic F, Lyubovitskij V E, Gutsche Th and Faessler A 2002 *Phys. Lett.* B **544** 121
Kitano R, Koike M and Okada Y 2002 *Preprint* hep-ph/0203110 see also references therein
[33] Volpe C and Kosmas T S in preparation